JETSET codes tests. Magnetic diffusivity

Miljenko Cemeljic 席門傑

TIARA (ASIAA, NTHU Hsinchu)

Colloquium in NCU, Nov. 02, 2007

Outline

- Introduction
- JETSET collaboration
- Test suites, “standard” tests
- Code tests beyond "standard"
- Resistive MHD test
- Prospects

Introduction

- Astrophysical media stretch use of codes: multicomponent, large gradients, viscosity, resistivity, chemistry included
- Few exact solutions, numerical solutions dependent on: numerical approximations, choice of i.c. and b.c. (initial conditions and boundary conditions)

Introduction

- Observations, more and more detailed, on various scales, put severe constraints to models and simulations.
- M-87, black hole powered jet of electrons and sub-atomic particles

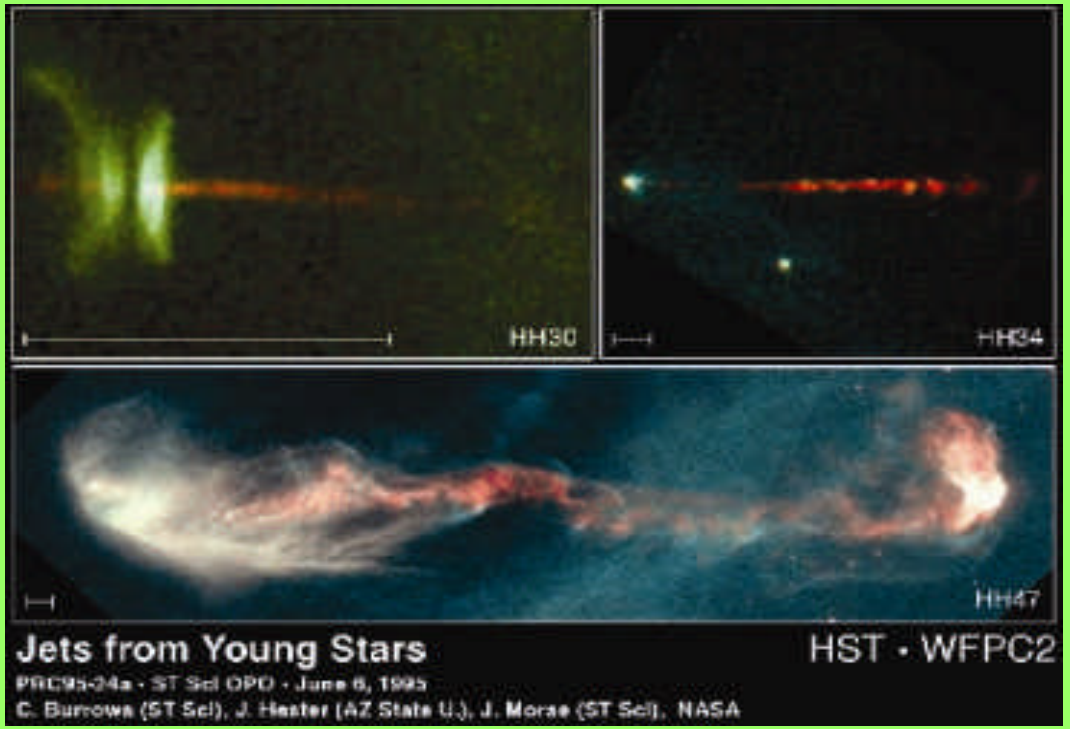

Introduction

- Laboratory experiments also illustrate how unusual, compared to everyday exeprience, astrophysical plasmas are.
- Here Z-pinch wire array, most powerful lab X-ray source.

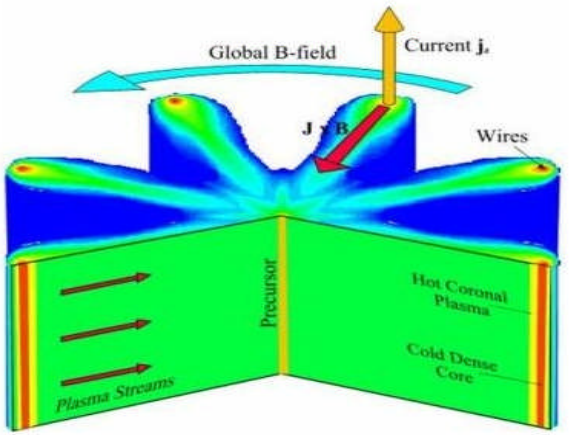

Upon arrival at the axis, the kinetic energy is transformed to thermal energy resulting in a plasma of very high temperature (~1keV) and density (~$1x10^{20}$ions/cm^3). The X-ray production in such plasmas is enormous, experiments at Sandia National Laboratory produce ~2MJ of X-rays with peak powers of ~290 TW. These X-ray pulses are used to energise hohlraums both for inertial confinement fusion experiments and as a testbed for experiments investigating the opacity of stellar material, the instabiiltiies of exploding supernovae and the equation of state of strongly coupled plasmas.

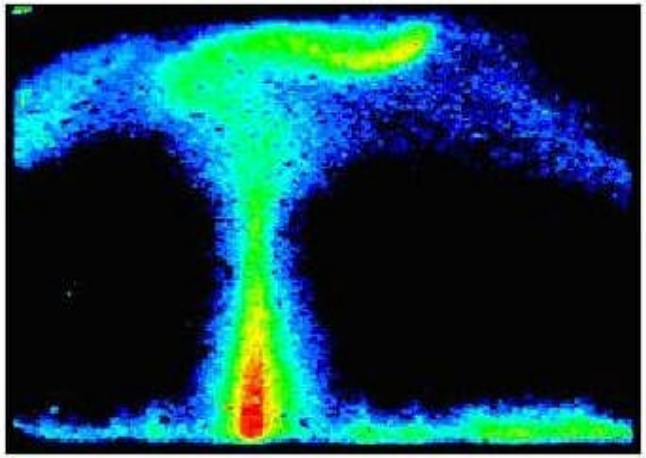

Figure 1. Soft x-ray image of a laboratory jet interacting with an Argon gas background and forming a bow shock.

Introduction

- PRECISE observations, and more precise to come
- HST; HH30 observations 1995-2000

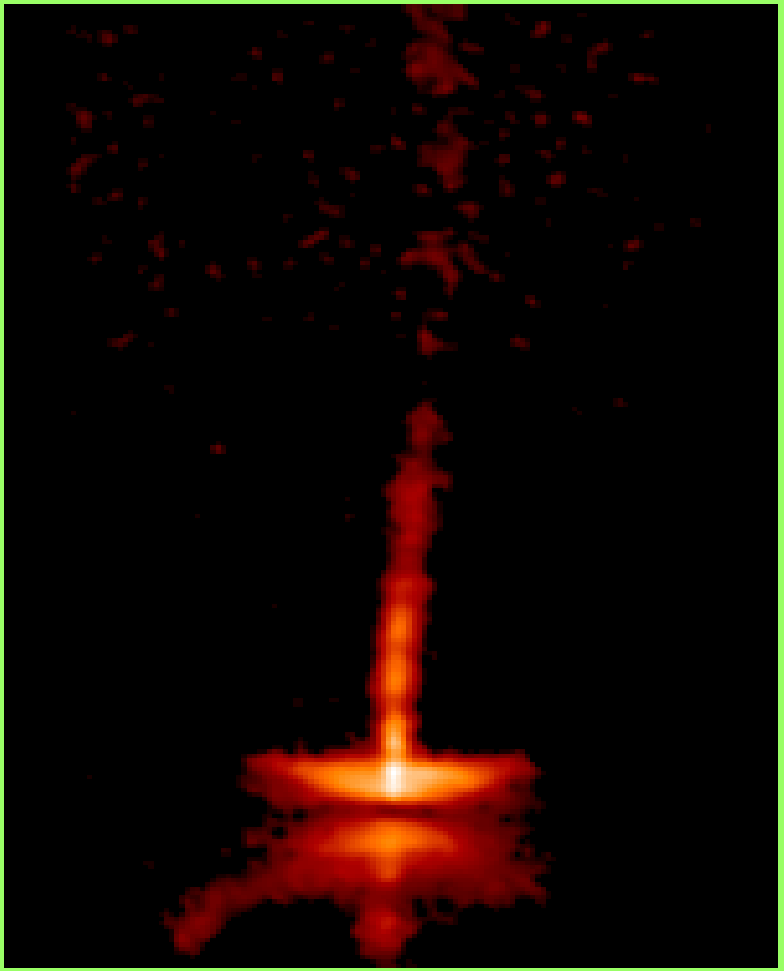

Introduction

- What we can simulate today?
- New codes, more powerful machines, we do our best!
- Machines versus codes:
  -faster machines, full 3D, larger comp. boxes
  -new numerical methods, “brutal force” in computing AND innovations

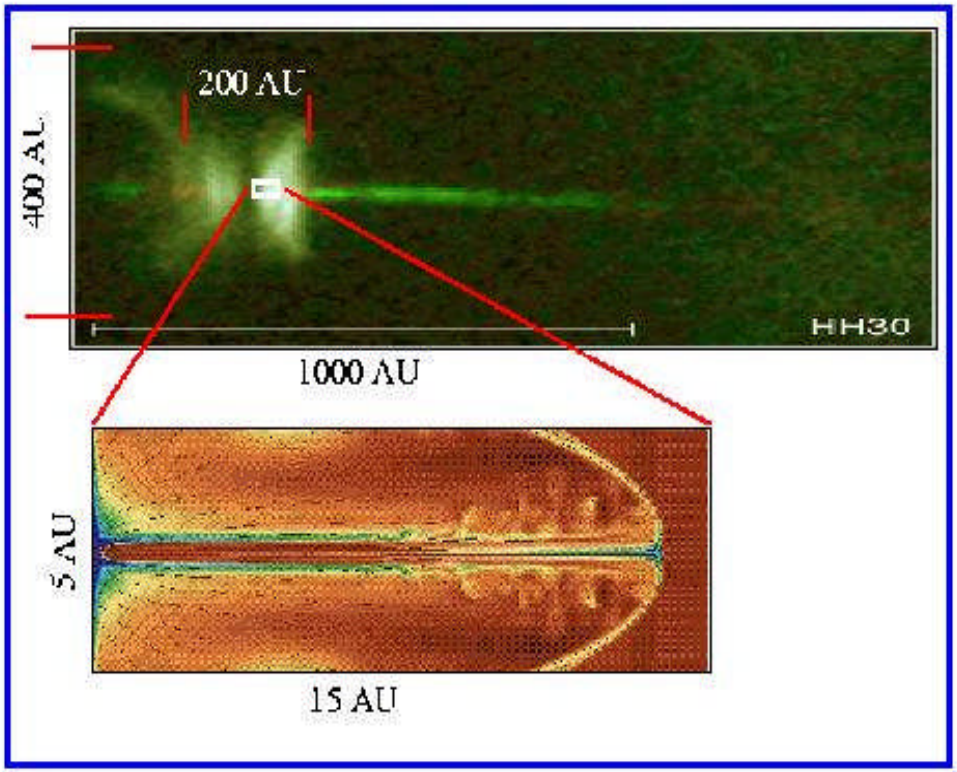

Introduction

- SuperHiperMegaGiga computer (“Deep Thought” ref.:Douglas Adams “The Hitchhiker's Guide to the Galaxy”) or shared computing (your work/home desktop? Laptop?)
  - dedicated linux cluster
  - Grid technology (similar to SETI idea)

Software 1

- **Codes** part 1
  - ZEUS (ZEUS3D) [LCA, NCSA David Clarke, Michael Norman, Robert Fiedler] MHD 3D + Molecular
  - 3DAthena-NASA [Stephen O'Sullivan] MHD 3D
  - AMRAthena (Zeus Team) [Tom Gardiner] MHD 3D
  - AMRVAC [Rony Keppens] MHD 3D
  - AMRAstroBear [Adam Frank + Peguy Varnieres]
  - 3DMHD SPH [E. Gouveia del Pino]
  - AMR [Andrew Lim]
  - Nirvana [Udo Ziegler]
  - TD code [Turlough Downes]
  - Hydra [Turlough Downes, Stephen O'Sullivan] Multi-Fluid MHD code
  - Flash [Chicago]

Software 2

- **Codes** part 2
  - Gorgon (Resistive MHD, on a fixed 3D eulerian grid,2 Temp + Q, LTE<Z> +Px), 2nd order hydro
  - Yguazu [Dublin, Raga + De Colle]
  - HyRas 3D hydro rad, cart/cyl/sph. euler, implicit solver
  - RAMSES, AMR HD multi-material gravity chemistry (CEA)(AMR + hydro + multi-Z EOS+ Chemistry)
  - Astrolabe 1D Radiative, multi-fluid, chemistry, gravity (CEA)(1D, hydro.rad, ALE multi-fluid (2 species and 2 temp.)
  - MULTI at Obspm
  - HR, 1 to 3D Eulerian cartesian (can be cylindrical or spheric),
  - grey (Rosseland) eulerian, implicit solver for R-T, gray with moments
  - Belenos (Sebastien Leygnac) 3D stationary Radiative Transfer(Exact 3D solution of radiative transfer equation) [DIAS-Cosmogrid]

Introduction-Numerical solutions

- Set of equations
  - ρ (density)
  - ρu (momentum)
  - ρe (energy)
  - B (magnetic field)
  - p (pressure)Numerical schemes (discretizations)

  - Numerical schemes differ in addressing the contact and shock discontinuities in the flow
  - overall accuracy depends on the way these problems are solved
  - finite differences, finite volume and finite elements method

Introduction-Finite differences method

- Use of neighbouring points: approximation of the derivative of an unknown quantity *U* at a grid point by the ratio of the difference in *U* at two adjacent points to the distance between the grid points.
  - mostly on regular mesh

Introduction-Finite volume method

- The variables are approximated by their average values in each volume, and the changes through the surfaces of each volume are approximated as a function of the variables in neighbouring volumes.
  - on both regular and irregular mesh

Introduction-Finite elements method

- Also splits up the spaces into small pieces (called *elements)* as in finite volume method. But now a grid point exchanges the information with all the other grid points with which it shares an element.
  - no advantage of regular mesh

- All this possible in AMR (adaptive mesh refinement) approach

JETSET collaboration tests

- Marie Curie RTN (Research and Training Network)
- December 2006, Dublin, initial workshop
- January 2007, final list of tests
- Up to end of 2007, webpage with posted tests and conditions for passing it

Test suites

- Example of “test suite”: problems which test a code thoroughly, all of the terms in equations. Each problem tests different MHD phenomenon, e.g. Stone et al. (1992):
- 1)Eulerian advection: tests advection of magnetic fluid
- 2)MHD Riemann problem:propagation of nonlinear compressive waves (shocks) and contact discontinuities
- 3)propagation of Alfven waves: propagation of noncompressive transverse waves
- 4)1.5D evolution of a stationary flow: overall dynamics
- 5)fully 2.5D dynamical problem with shocks: overall dynamics

Test suites: Eulerian advection

Advection of a square pulse of transverse mag. field originally 50 zones wide a distance of 5 times its width. Donor cell, van Leer and PPA interpolation methods. Analytic locations of field discontinuity are at 0.4 and 0.6

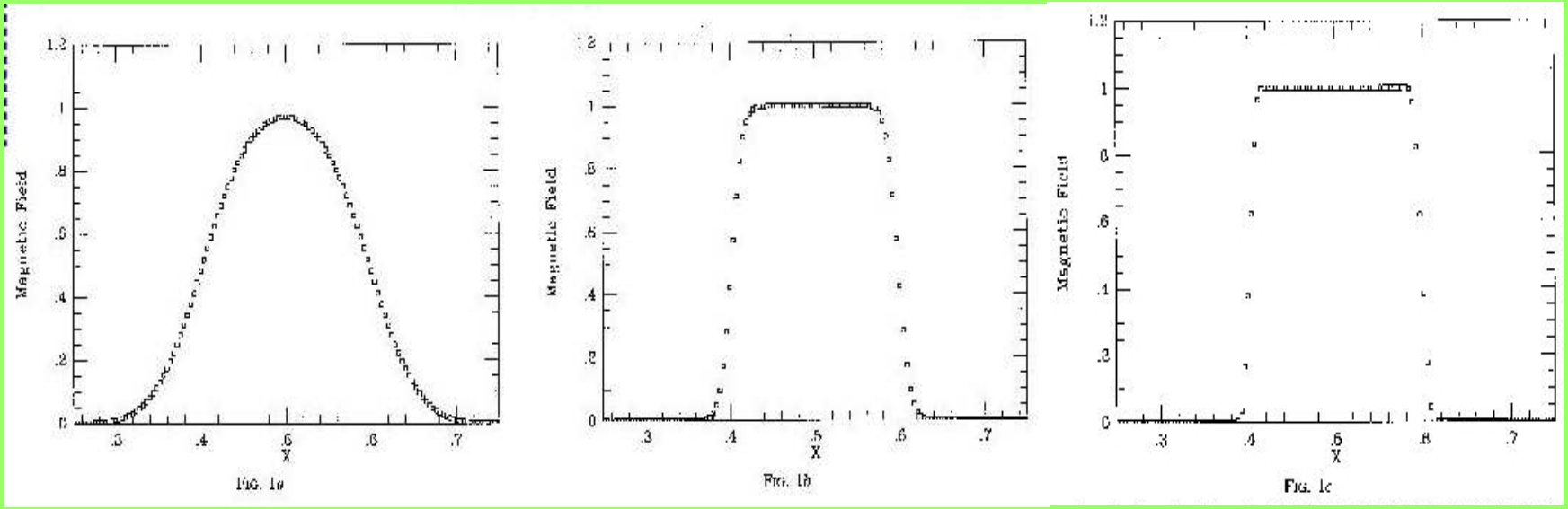

Test suites: Eulerian advection

Current density for the square field pulse computations. Analytic
solution is delta function at x=0.4. PPA, van Leer and donor cell
give increasingly broader solutions.

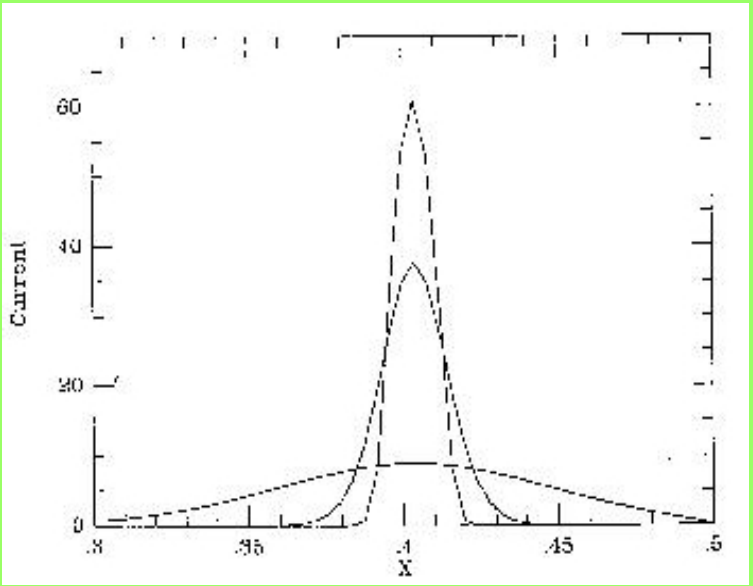

Error for advection test, as a function of spatial location x. PPA, van Leer and donor cell give increasingly larger error.

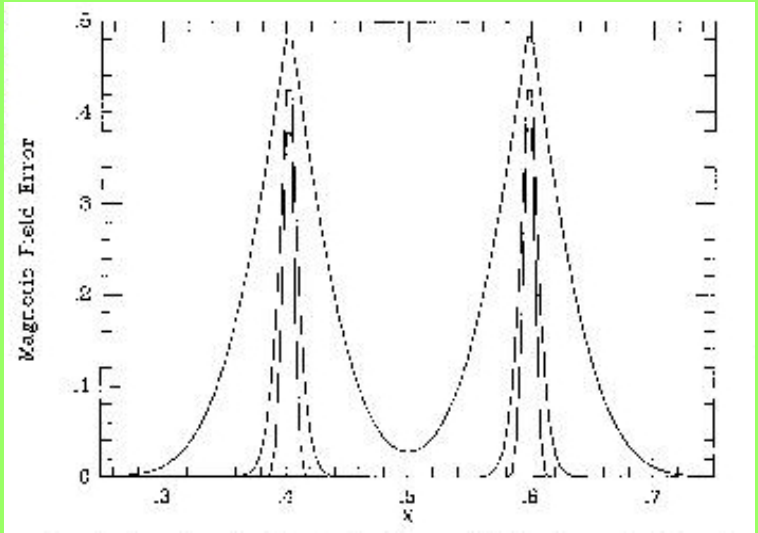

Test suites: MHD Riemann problem-shock capturing methods

- Classical
  - linear numerical dissipation terms
  - the same dissipation at all grid points
  - for smooth and weak-shock solutions
  - symmetric or central discretization
  - no info used about wave propagation
- *and* modern method
  - non-linear numerical dissipation
  - feedback for adjusting of dissipation
  - every cell adjusted
  - based on “upwind differences” (PDEs solutions dependent on velocity sign)
- *intermediate method*
  - linear numerical dissipation terms, non-linear switch functions

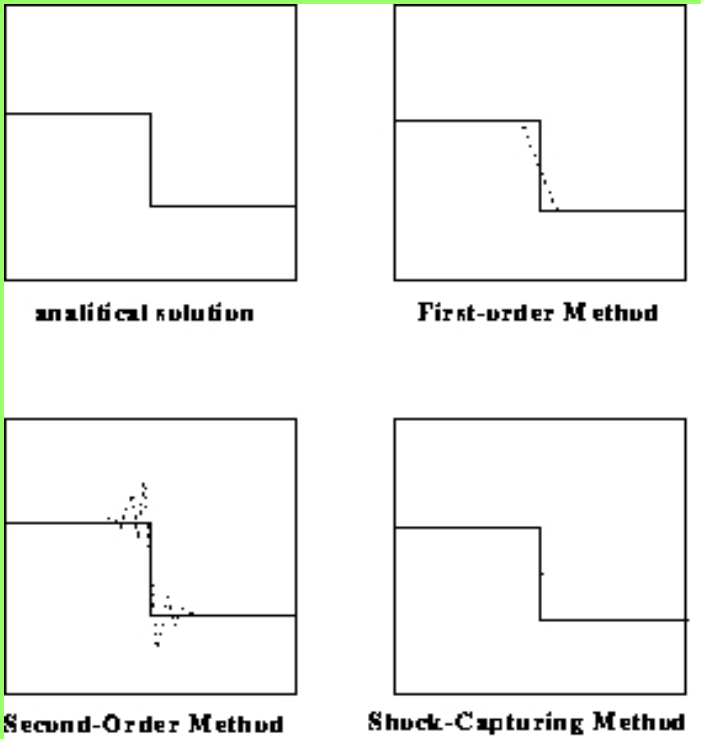

FIG. 2. *Examples of numerical discretizations*

Test suites: MHD Riemann problem

- in HD-the simplest initial value problem
  - discontinuous data
  - two separated constant states
  - breakup of discontinuity
  - two types of waves:
  - shocks *and* rarefactions
  - contact discontinuity (moving)

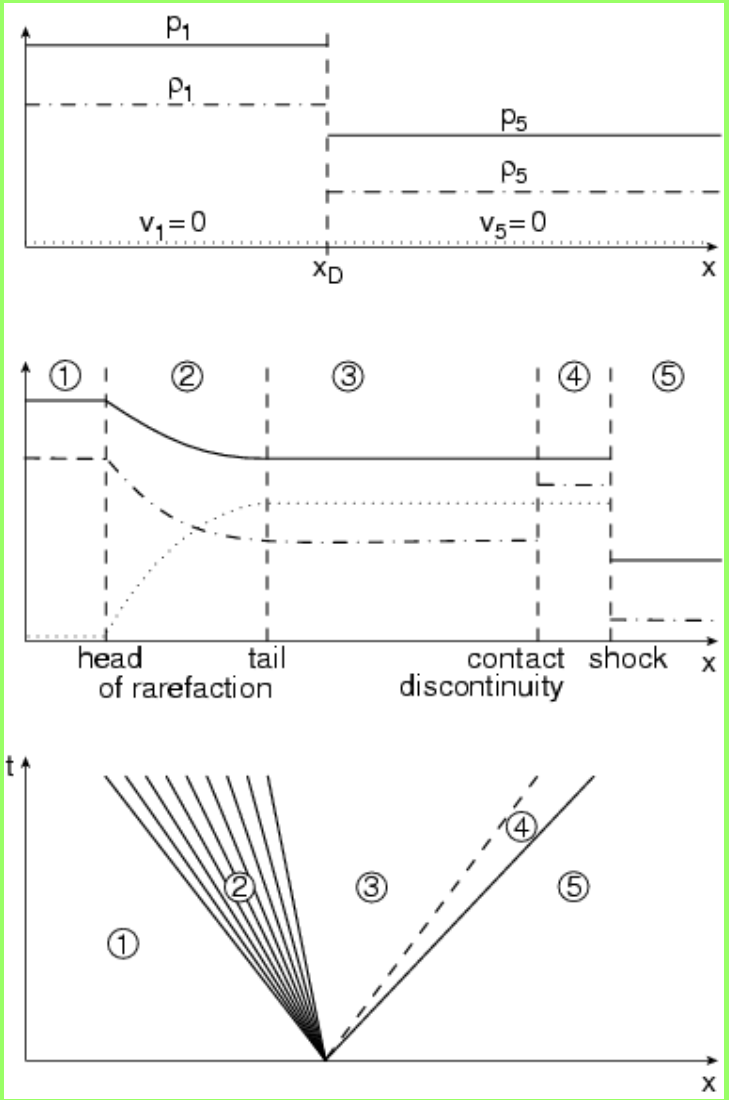

Test suites: MHD Riemann problem-Godunov type schemes

Godunov (1959) exact Riemann solver

-solving of a separate Riemann problems

-solving at each cell boundary

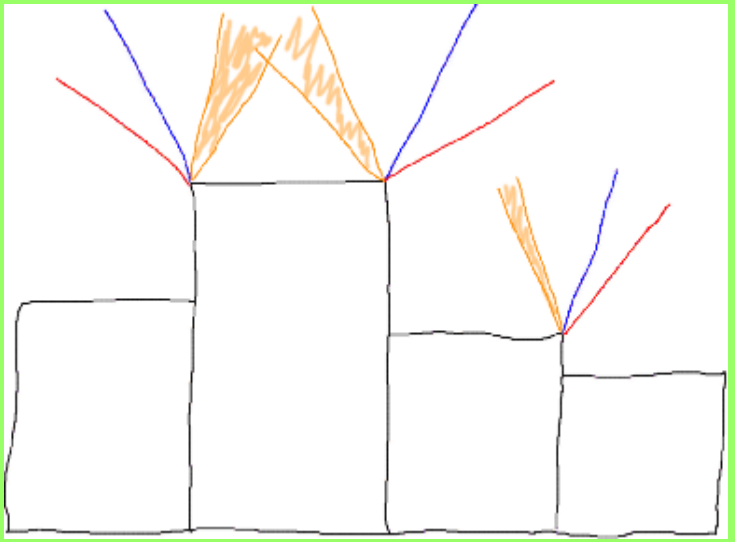

- **Three steps (*U*=1,v,e):**
  - reconstruction of ρU(x) from cell ρU-es
  - solving of Riemann problems for Δt
  - computing the fluxes across cell boundaries and averaging of ρU(x)-es to obtain ρU-es
- *Useful method, but in original form too diffusive*

Test suites: Riemann problem-Riemann solvers

- *What is usually used is combination of Godunov's concept with high-order reconstruction (solution averaging):*
  - Van Leer (1979): MUSCL (Monotone Upwind Schemes for Scalar Conservation Laws)-linear reconstruction: approximation of piecewise-linear Riemann problems by piecewise-constant Riemann problems including slope-limiter, solution of the Lagrange equations and Eulerian remapping.
  - Colella & Woodward (1984): PPM (Piecewise Parabolic Method): piecewise parabolic reconstruction via primitive functions, contact steepening.
  - Approximate (linearized) Riemann solvers may serve as well in splitting the flow into waves with different characteristic velocities and upwind directions.

Test suites: MHD Riemann problem-alternatives

- *(Approximate) Riemann solvers account for upwinding and shock capturing but:*
  - involved computations, costly in CPU time
- Alternatives-simpler-make use of:
  - von Neumann-Richtmyer viscosity
  - Runge-Kutta steps
  - operator-splitting of advection and pressure terms
- Other Riemann solvers:
  - Approximate Riemann Solver of Roe (1981)-solves exactly a linearised problem (by an algorithm by Roe), instead of looking for an iterative solution of the exact original Riemann problem
  - Harten-Lax-van Leer-Einfeldt (or HLLE) scheme (1988)-the energy of a flow is highly kinetic

Test suites: MHD Riemann problem

1D fully dynamical problem. Type of it is often referred “shock tube problem”, Sod (1978), which is “standard” test in HD. In MHD: Brio & Wu (1988) magnetic Riemann problem, demonstrates nonconvexity of the MHD eqs. It tests the ability of num. scheme tosolve shocks, rarefactions and waves in MHD flows.

Here is pressure profile, magnetic field is similar.

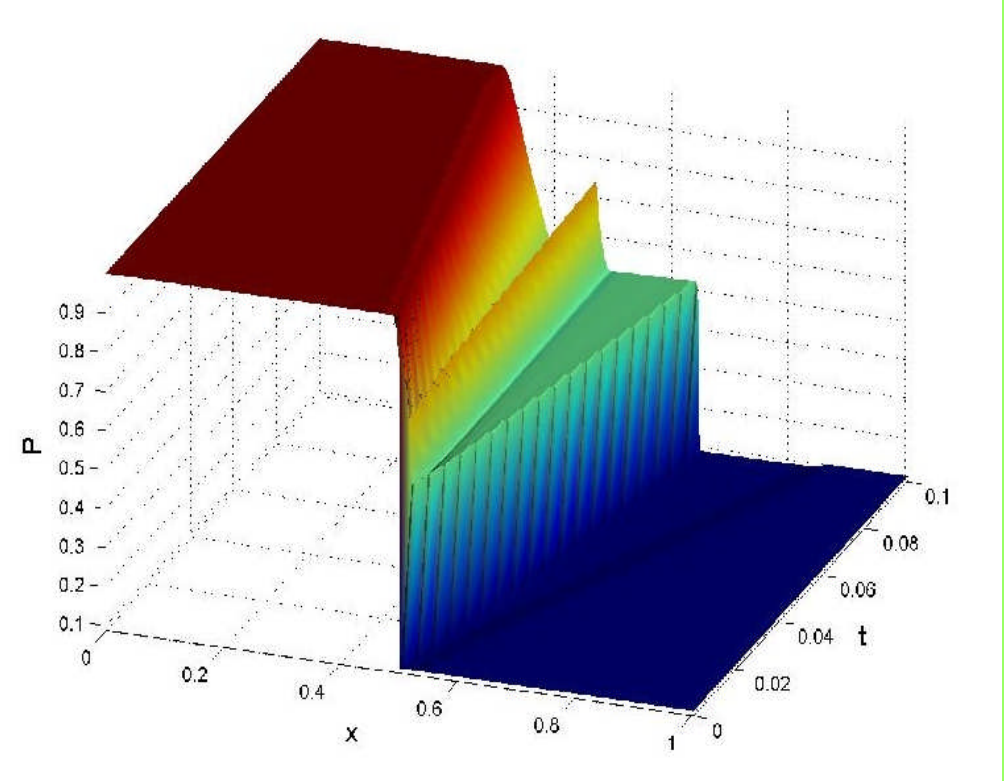

Test suites: Propagation of Alfven waves

These waves are unique to MHD.
As a test: comparison with analytical solutions for the magnetic braking of an aligned rotator (Mouschovias & Paleologou, 1980)
Physically: time evolution of a rotating cylinder of dense gas, embedded in a homogeneous ambient medium and threaded by a uniform axial magnetic field. The shear at the disk surface generates A. waves which propagate along the meg. field lines into the amb. medium (accelerating it) and disk (decelerating it). Rotational velocity v_ φ and B_φ are compared with analytical solution.

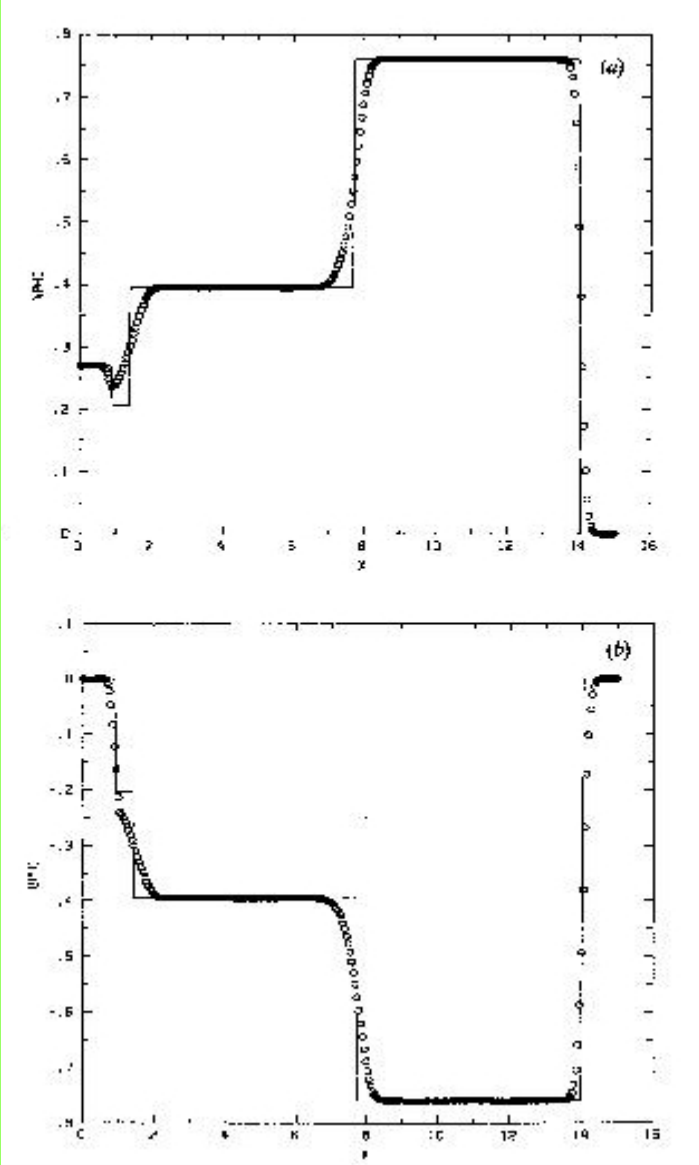

Test suites: 1.5D evolution of stationary flow

Steady 1D magnetized wind solution; Weber & Davis (1967) [assumes B_p geometry purely radial]. 2D solutions by Sakurai (1985).

Solution can be exploited multiple ways.

1)set complete analytical solution in the grid and compare evolution of it with the initial state=direct measure of the truncation error.

Single timestep is enough!

Also, setup of inflow b.c. and its evolution to stationary state, and then comparison with analytical solution, is possible.

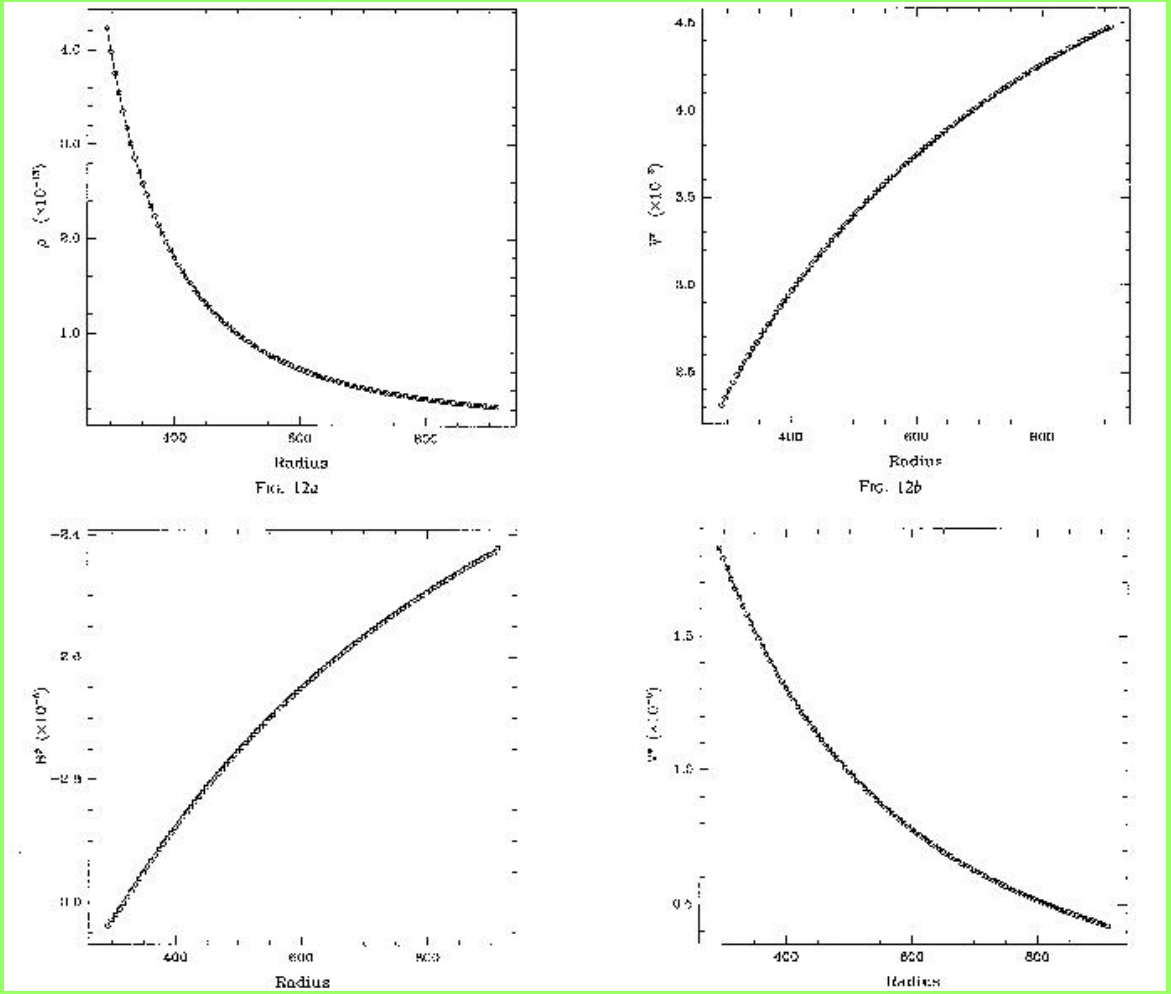

Test suites: 2.5D evolution of flow with shocks

Solar coronal transients (Low, 1984)
-violent expulsion of hot magnetized bubble into a spherically symmetric nonmagnetic ambient.

Run of analytic (time dependent) solution is set, and evolution followed. Direct comparison is used to compute errors. These are then showed, and analyzed.

Top panel are density isocontours (solid) and poloidal mag. field lines (dashed), bottom panel are isocontours of B_φ. Times shown are 0.874,1,75 and 2.62 x10^4 sec.

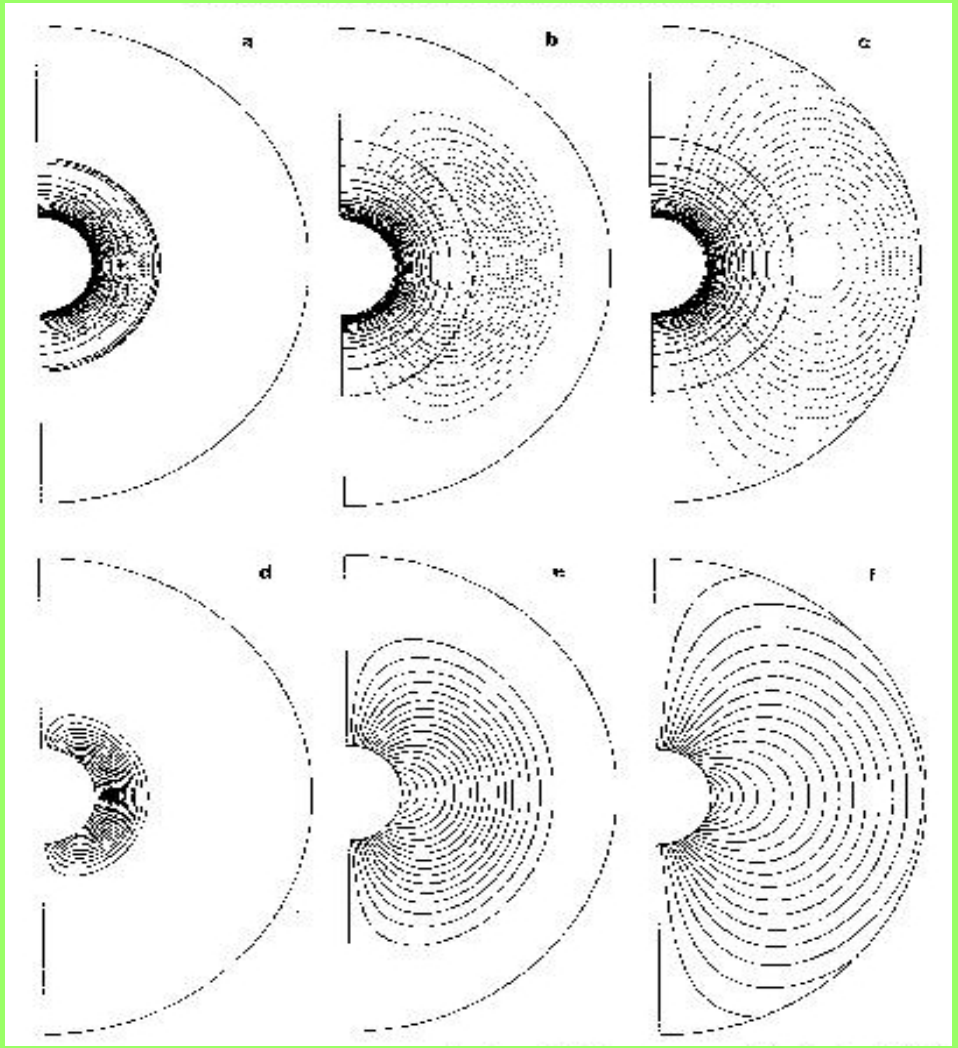

Test suites: 2.5D evolution of flow with shocks

Error analysis. Relative errors in the density (0.98%), radial velocity (0.98%), radial magnetic field (2.6%) and toroidal magnetic field (2.1%).

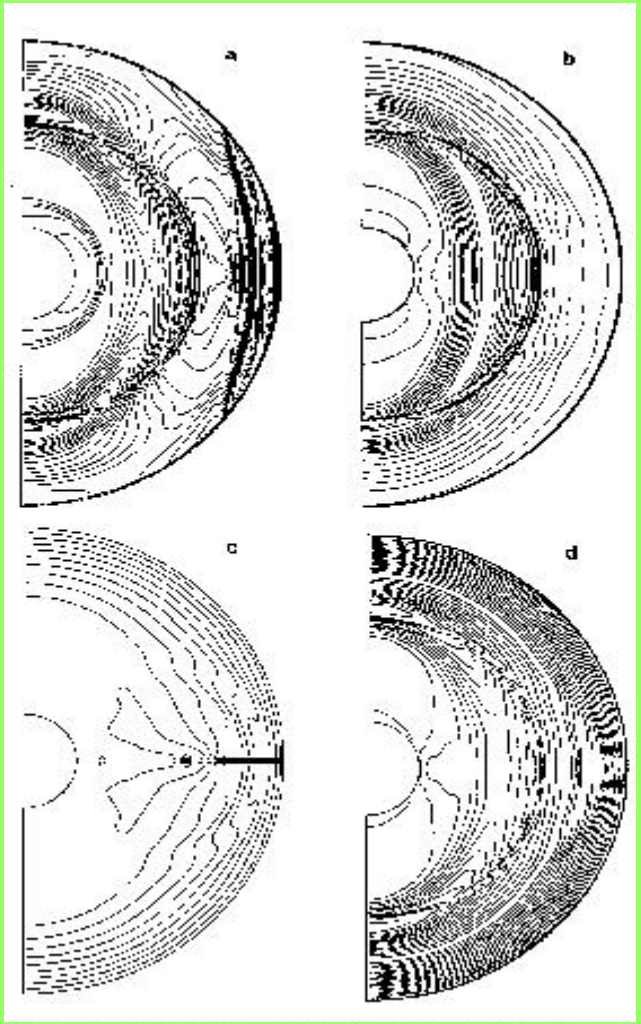

JETSET tests

- Advection of a current-carrying cylinder
- Orszag-Tang Vortex
- MHD Kelvin-Helmholtz Instability
- Under-expanded Jet
- Double Mach Reflection of a Strong Shock
- Oscillatory Instability of Radiative Shocks
- -Magnetic Blast Wave propagation
- -Cloud-Shock Interaction
- Magnetic diffusion

Advection of a current-carrying cylinder

- introduced by deVore 1991, tests divB=0
- 2D, cartesian, (x,y)=(200,100)pts
- initial setup:

$$\begin{cases} \rho = p = 1 & v_x = 2 & v_y = 1 & A_z = A_0(r_0 - r) & \text{if } r \le r_0 \\ \rho = p = 1 & v_x = 2 & v_y = 1 & A_z = 0 & \text{if } r > r_0 \end{cases}$$

- Evaluation:
  -exact solution known
  -images

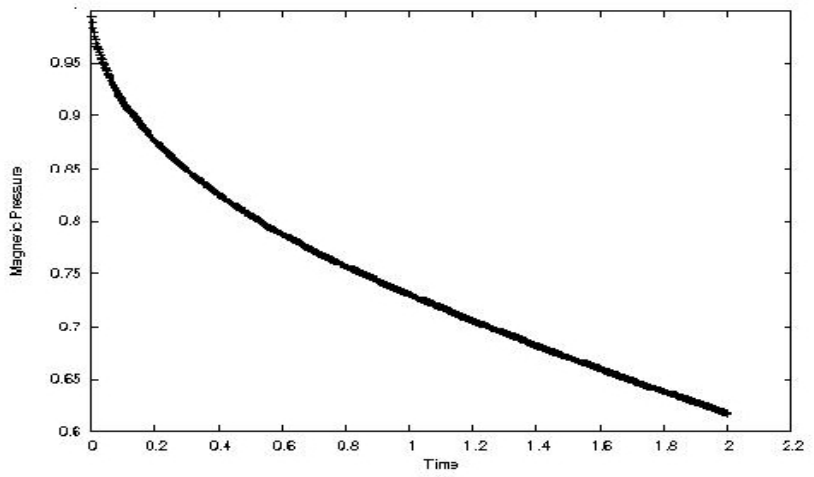

Figure 1: Magnetic pressure evolution in time

Advection ...

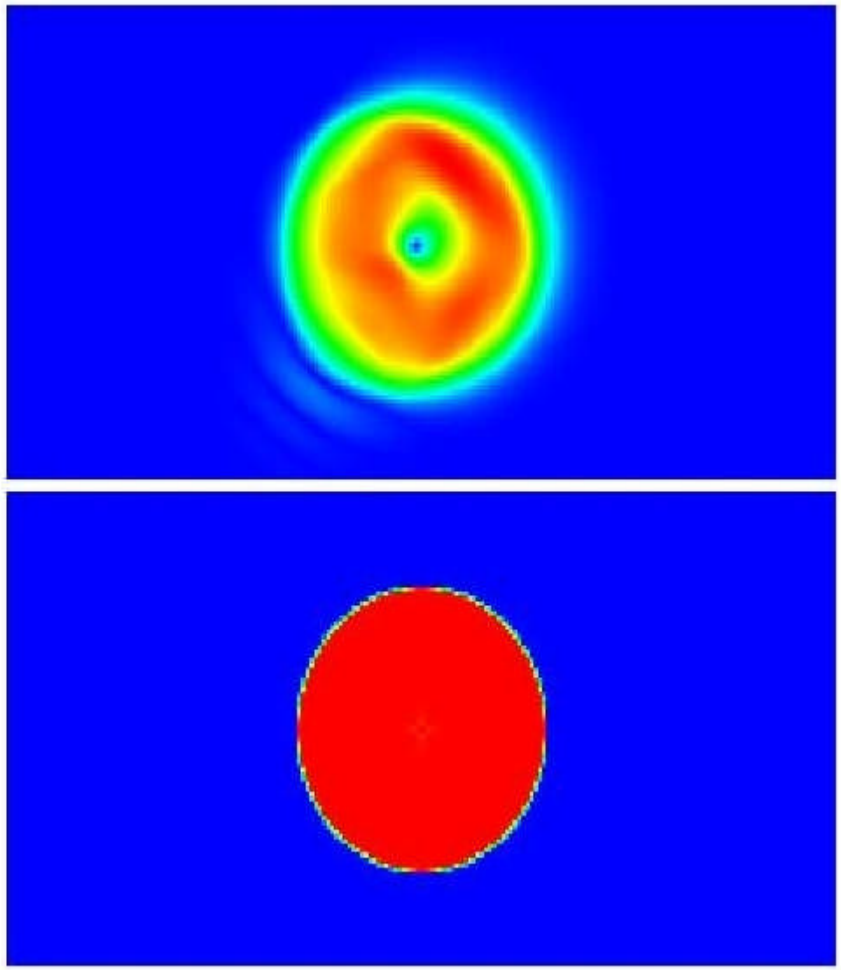

Figure 2: Magnetic pressure at the initial (lower panel) and final (upper panel) time

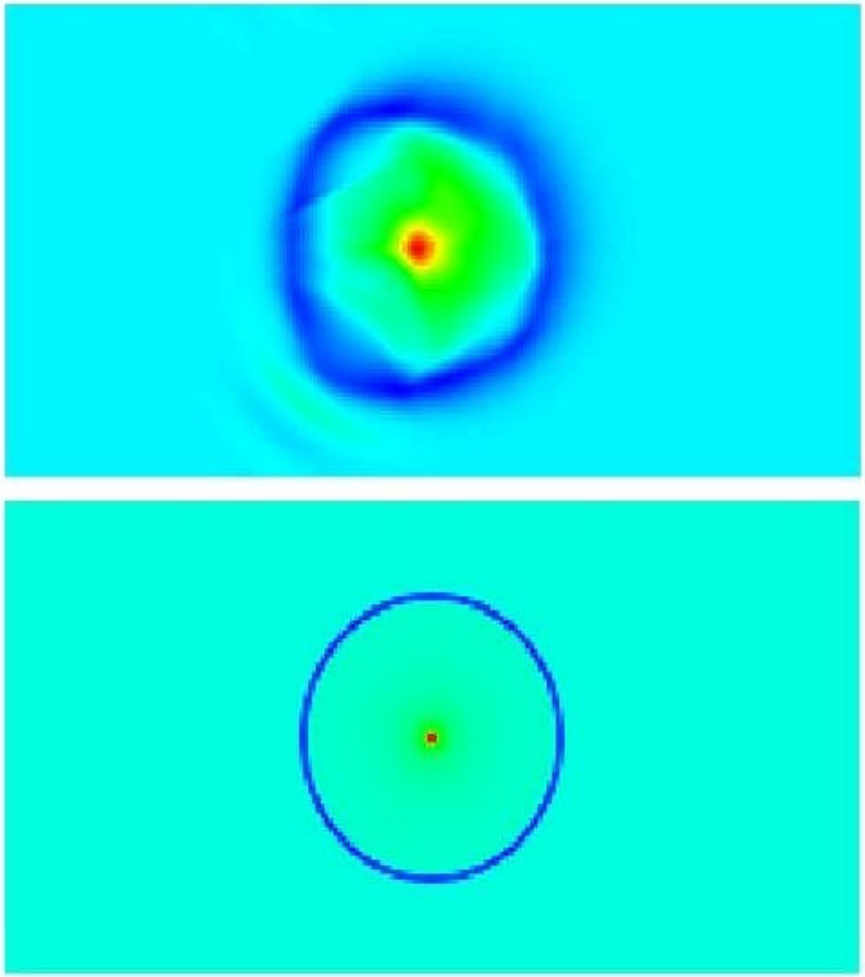

Figure 3: Density current $\vec{J}$ at the initial (lower panel) and final (upper panel) time

2D compressible MHD vortex of Orszag & Tang

- by O&T 1979, test if code can handle shocks in two dimensions, also divB=0 test.
- initial conditions vary in literature, here we set:
- no analytical solution, qualitative comparison of 2D plots and 1D cuts of density, vorticity (rot v) , compressibility (div v), divB, temperature, thermal and magnetic pressure, with other solutions. Different divB=0 schemes produce slightly different results.

$$U = \begin{pmatrix} \rho = \frac{25}{36\pi} \\ v_x = -\sin(2\pi y) \\ v_y = \sin(2\pi x) \\ v_z = 0 \\ B_x = -\sin(2\pi y) \\ B_y = \sin(4\pi x) \\ B_z = 0 \\ p = \frac{5}{12\pi} \end{pmatrix}$$

Orszag & Tang

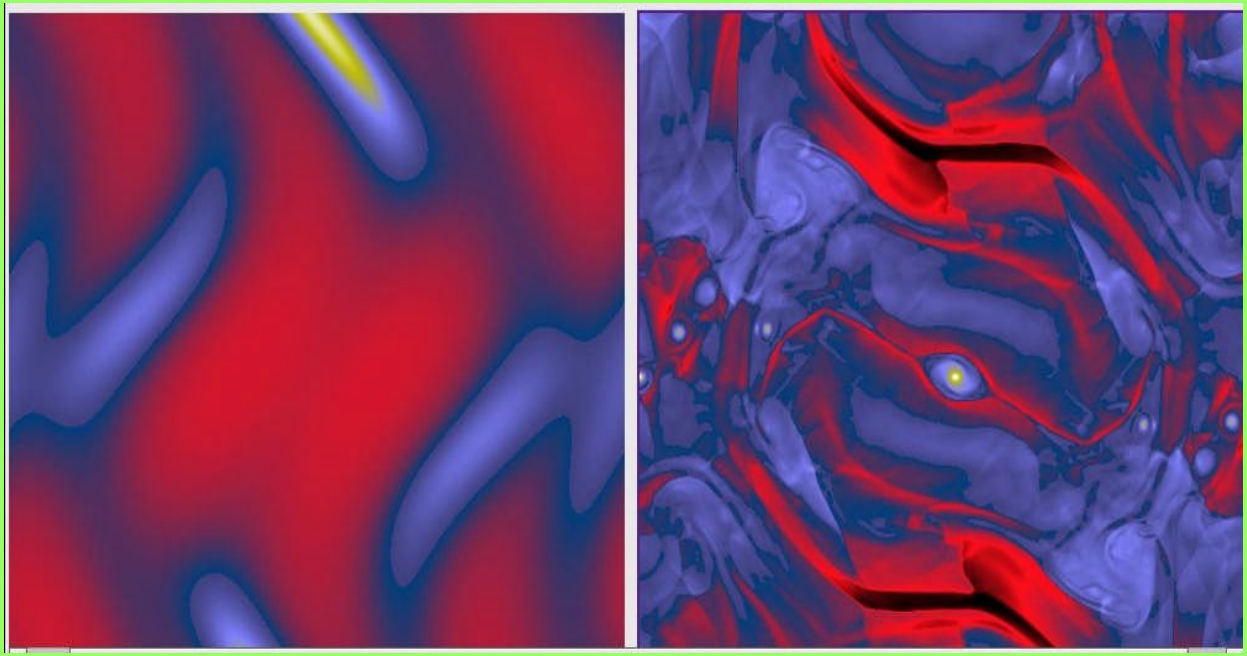

Orszag & Tang

MHD Kevin-Helmholtz instability

– based on Miura & Pritchett (1982) results, introduced by Keppens et al. (1999); test verifies the general behavior of KH instability in a magnetized plasma, and checks if code can reproduce correctly the linear phase of instability.

– Initial conditions: Bx=Bo, By=0, take care of b.c., take ca about “outflow” b.c.

– Evaluation:
-growth rates
general behavior

$$\rho = 1 \qquad p = 1/\gamma$$

$$v_x = 0.5 \cdot M \cdot \tanh(y/a)$$

$$v_y = 0.01 \cdot \sin(2\pi x) \cdot exp\left(\frac{x}{4a}\right)^2$$

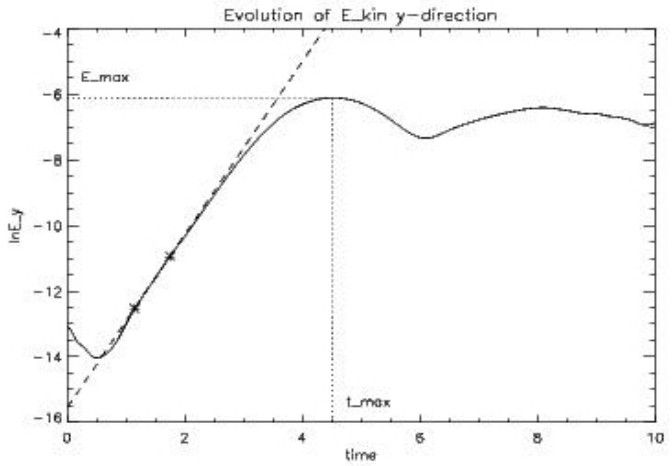

Figure 1: Logarithmic plot of the total kinetic energy along the y direction. Also shown are the saturation level E Max and the corresponding time t Max. The growth rate of the instability is obtained from the linear fit in the interval [0.25t Max, 0.4t Max], represented by the dashed line.

MHD KH

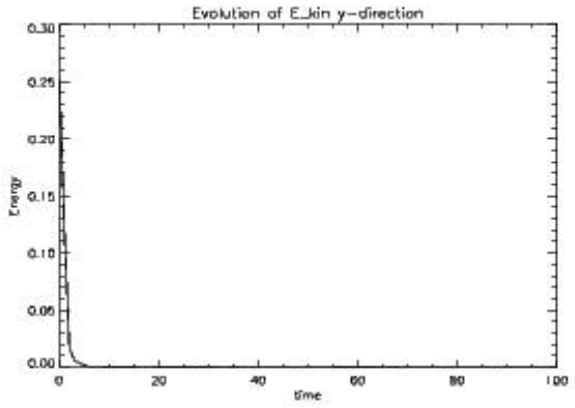

Figure 2: Total energy evolution in the case of Alfvén Mach number = 1.

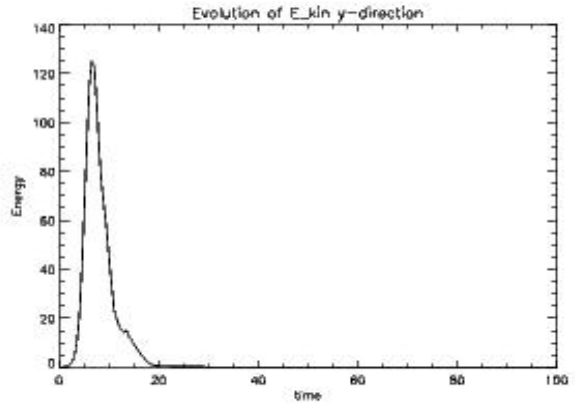

Figure 3: Total energy evolution in the case of Alfvén Mach number = 3.

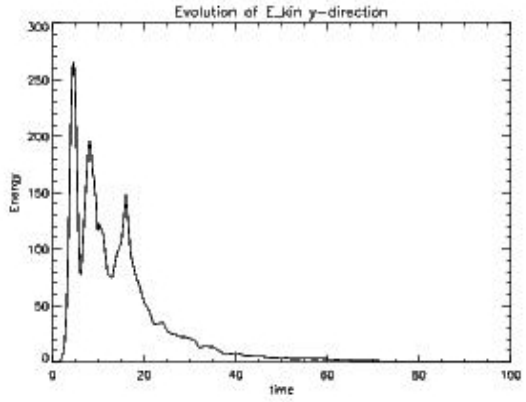

Figure 4: Total energy evolution in the case of Alfvén Mach number = 10.

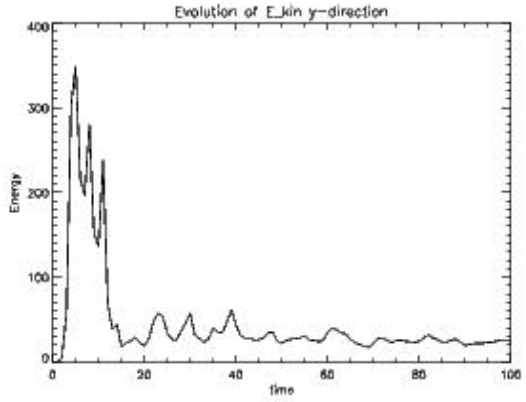

Figure 5: Total energy evolution in the case of Alfvén Mach number = 40.

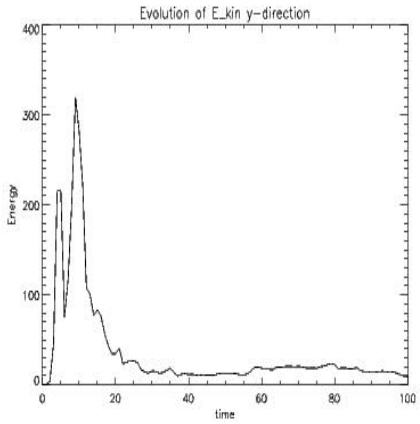

Figure 9: Total energy evolution in the case of Alfvén Mach number = 10, using the eight waves method for the divergence of B.

MHD KH....

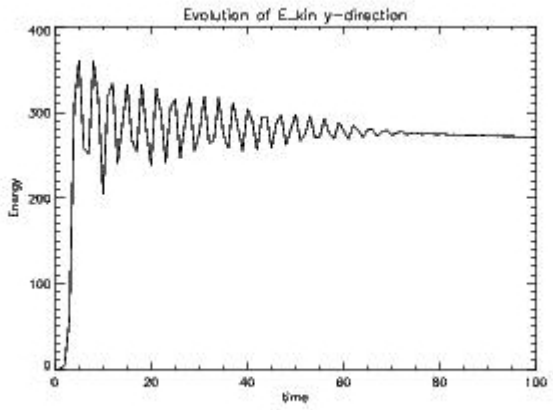

Figure 6: Total energy evolution for a pure hydrodynamic case.

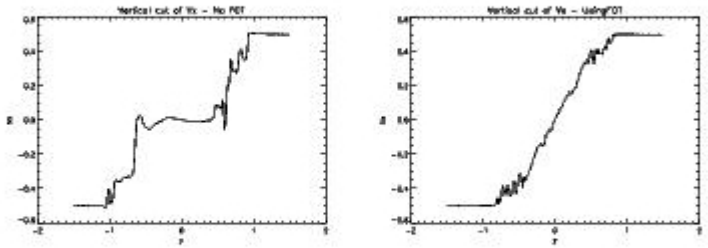

Figure 7: *Left*. Velocity along x direction in the case of Alfvén Mach number = 10, at the end of the simulation: cut along a vertical line x=0.5. Eight waves method was used to treat divergence of B. *Right*. Same as the Left image, but using FluxCT method.

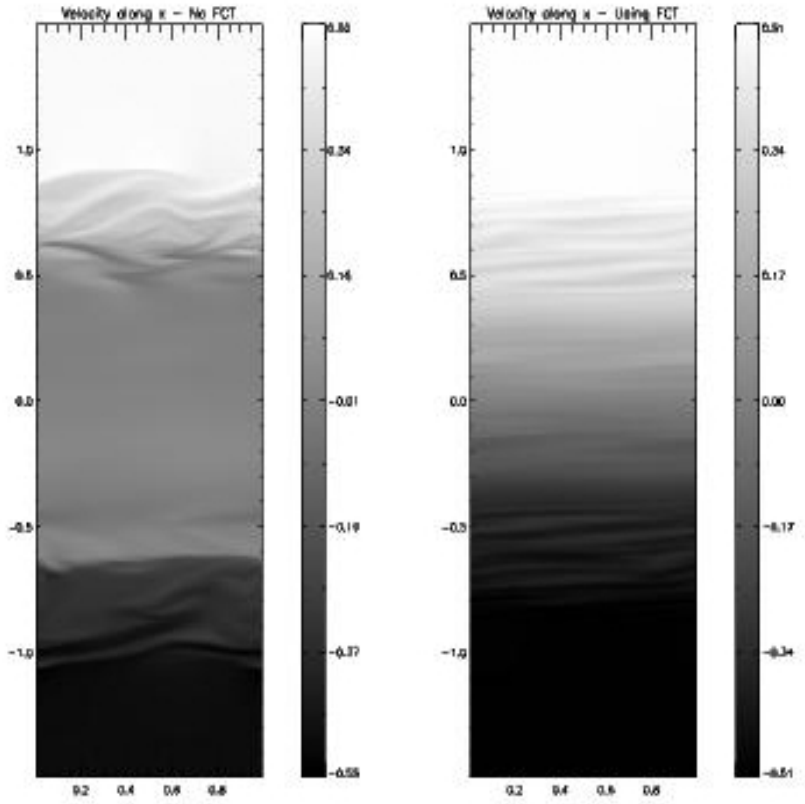

Figure 8: *Left*. Velocity along x direction in the case of Alfvén Mach number = 10, at the end of the simulation. Eight waves method was used to treat divergence of B. *Right*. Same as the Left image, but using FluxCT method.

Under-expanded jet

- Mignone, 2007; comparison with laboratory experiment
- injecting gas at p_0 through a nozzle into chamber under low pressure p_c (shock!)
- empirical expression:

$$z_{\rm m} = 1.34\, r^* \sqrt{\frac{p_0}{p_{\rm c}}}\,, \tag{1}$$

with r^* the effective sonic nozzle radius. Furthermore, Knuth (1964) obtained for the Mach number $M_{\rm axis}$ on the jet axis the following empirical expression:

$$M_{\rm axis} \approx (2.2)^{\frac{\Gamma-1}{2}} \left[\Gamma(\Gamma-1)\right]^{-\frac{\Gamma-1}{4}} \left(\frac{\Gamma+1}{\Gamma-1}\right)^{\frac{\Gamma+1}{4}} \left(\frac{z}{2r^*}\right)^{\Gamma-1}. \tag{2}$$

We have carried out 2D numerical simulations in cylindrical coordinates on a uniform grid $r \in [0,40]$, $z \in [0,80]$ with 20 zones per beam radius. The grid has been further extended in both directions (up to $r = 80$ and $z = 160$) by adding a second patch of geometrically stretched zones (100 and 200 zones in r and z, respectively) in order to avoid spurious reflections at the boundaries. Free outflow is set at the outer boundaries and reflective conditions are imposed on the axis $r = 0$ and for $r > 1$ at $z = 0$. Considering the actual nozzle as the injection zone at $z = 0$, $r \le 1$, we have obtained the values of the pressure p^* and density ρ^* by employing the isentropic laws for a perfect gas (Shames 1983) for a converging nozzle with stagnation pressure p_0 and density ρ_0:

$$p^* = p_0 \left(\frac{2}{\Gamma+1}\right)^{\frac{\Gamma}{\Gamma-1}}, \quad \rho^* = \rho_0 \left(\frac{2}{\Gamma+1}\right)^{\frac{1}{\Gamma-1}}. \tag{3}$$

Under-expanded jet

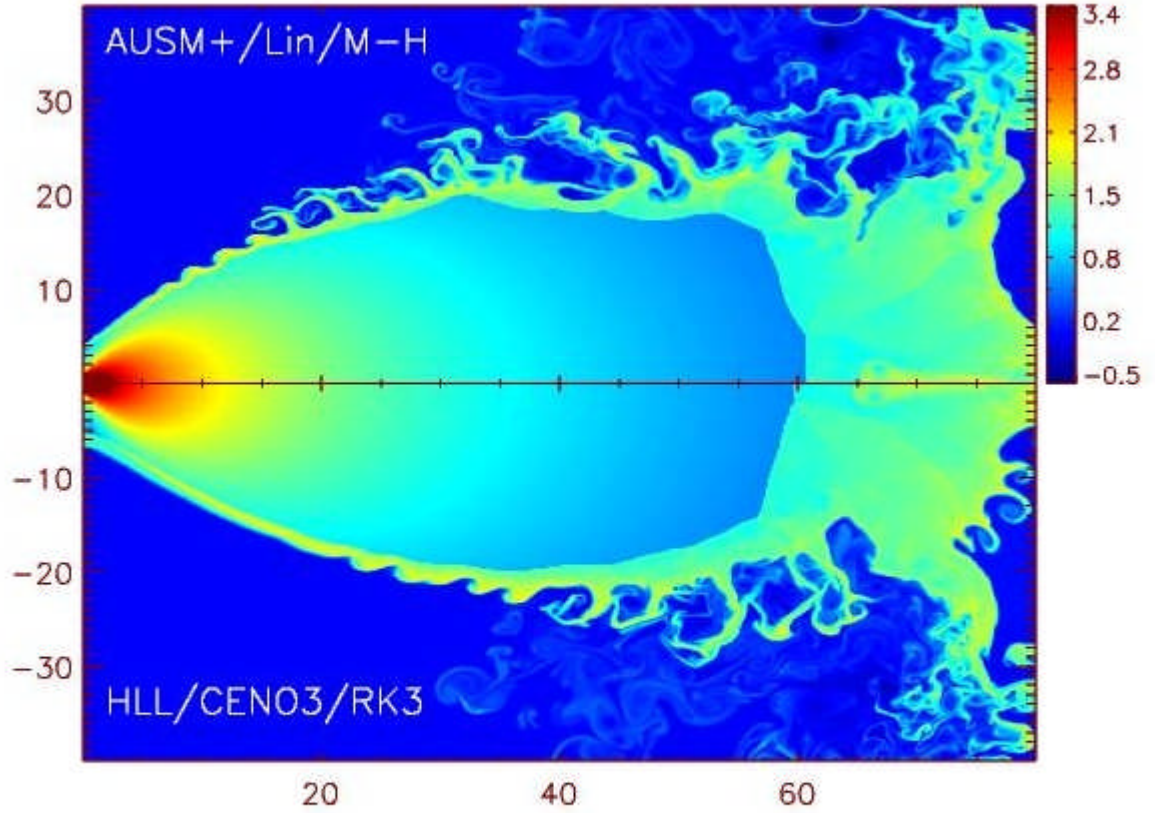

Figure 1: Density logarithms for the under-expanded jet at $t = 240$, for the linear Muscl-Hancock CTU with the AUSM+ solver (top) and the RK3 with HLL solver and third-order CENO interpolation (bottom).

Under-expanded jet

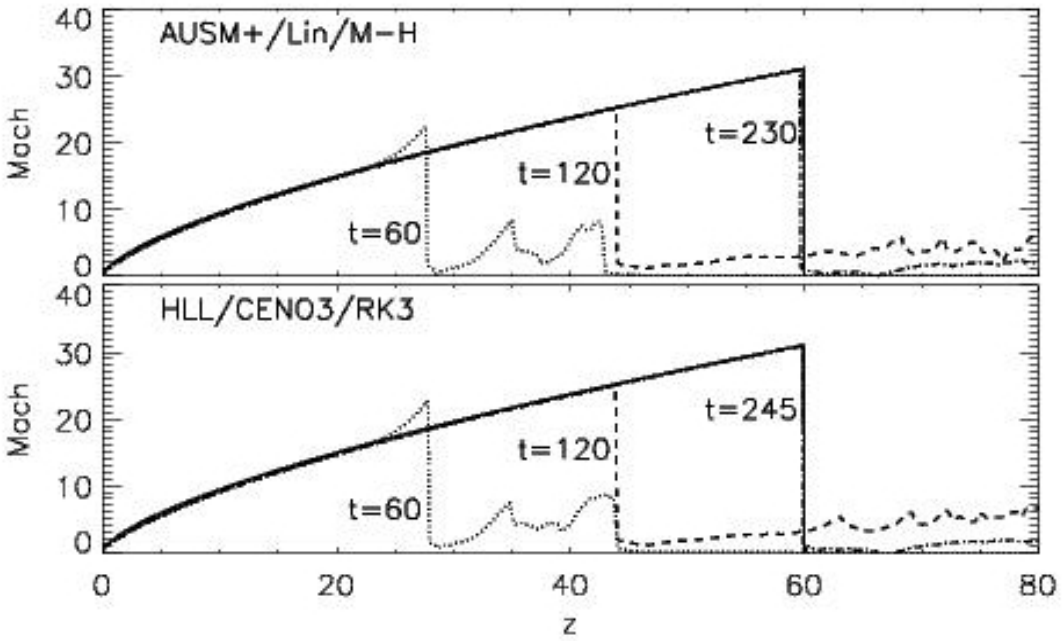

Figure 2: Axial Mach numbers plotted at $t = 60, 120, 230$ (for Muscl Hancock) and at $t = 60, 120, 245$ (for RK3) using dotted, dashed and dash-dotted lines, respectively. Because of the small-amplitude oscillations around the equilibrium position, the last time is not the same. The solid line gives the empirical relation (2) for $0 < z < z_m$ where z_m is given by Eq. (1).

Double Mach reflection of a strong shock

– Woodward & Colella (1984), test for reflection of a planar shock under an angle with a re wall.

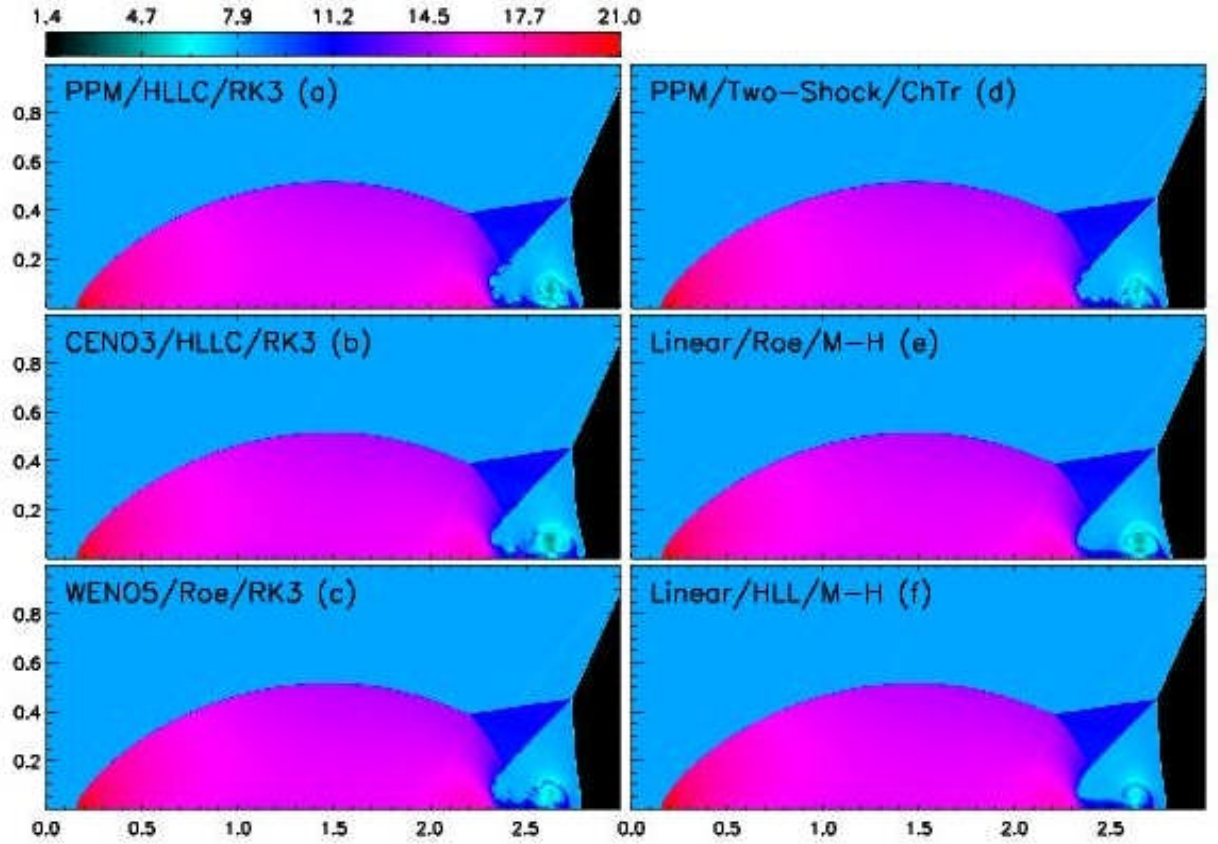

Figure 1: Density maps for the double Mach reflection test at $t = 0.2$. Each panel shows results obtained with the different combinations of schemes listed in table 1. The mesh size ($1/\Delta x = 1/\Delta y = 480$) and Courant number ($C_a = 0.8$) are the same for all cases. For the sake of clarity only the region $[0, 3] \times [0, 1]$ is shown.

Oscillatory instability in radiative shocks

- Mignone, 2005; steady state solution used as initial condition, and boundary-induced oscillations perturb the shock. Test for the energy budget of the system-reproducing the expected oscillations of the shock.
- 1D cartesian grid, HD equations +cooling. Nontrivial post-shock state. Also some compromises in the setup, for simplicity.
- Evaluation: 1)position of the shock, 2)power spectrum of the shock with peak at fundamental mode

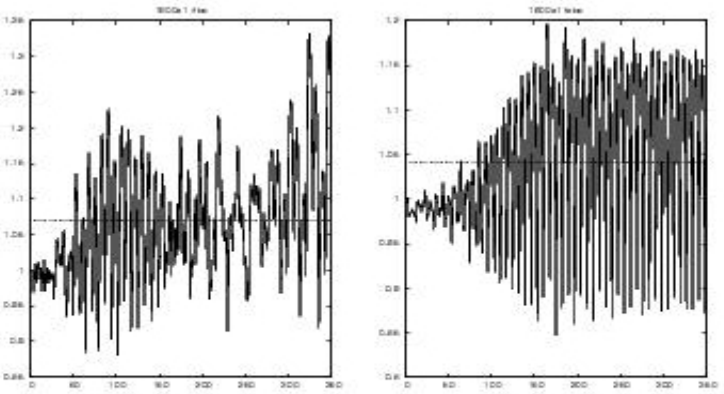

Figure 3: *Left: Time series plot of the shock position with a resolution of 1600x1, and with normal reflective boundary conditions Right: Time series for the case of the fixed boundary condition.*

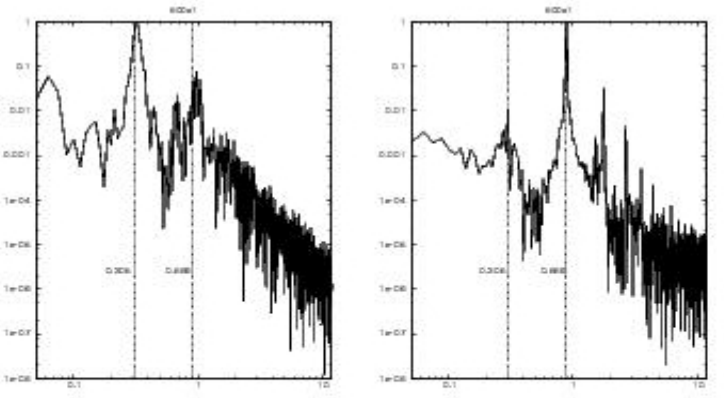

Figure 4: *Left: Normalised power spectrum of the time series of the shock position versus angular frequency from a simulation with a resolution of 800x1, and with normal reflective boundary conditions Right: The power spectrum for a simulation with a fixed condition for the flow variables at the wall. In both cases the fundamental ($\omega = 0.305$) and first ($\omega = 0.889$) modes are indicated by the dashed lines.*

Oscillatory instability...

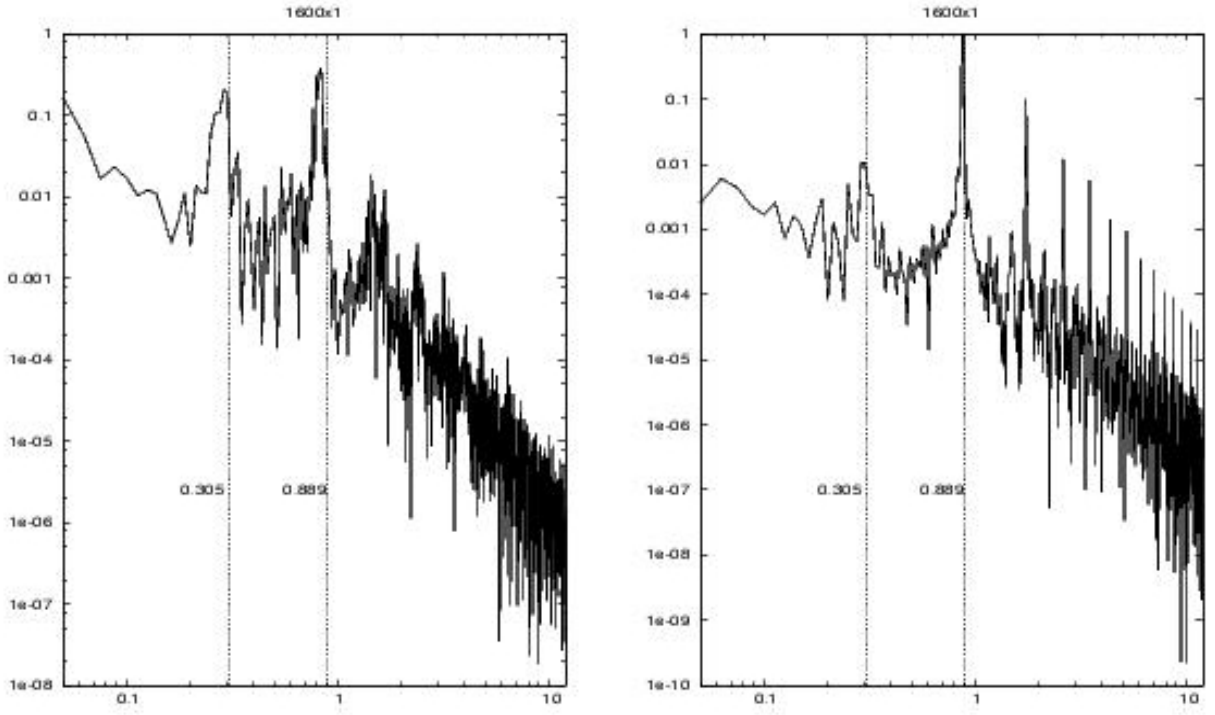

Figure 5: *Left: Normalised power spectrum of the time series of the shock position from a simulation with a resolution of 1600x1, and with normal reflective boundary conditions Right: The power spectrum for a simulation with a fixed condition for the flow variables at the wall. In both cases the fundamental ($\omega = 0.305$) and first ($\omega = 0.889$) modes are indicated by the dashed lines*

Magnetic diffusion test

- Disk as a boundary condition
  - **Ideal** MHD, Ouyed & Pudritz, 1997
- Time-dependent **resistive** MHD simulations-**ZEUS347, open field threading the disk,** Fendt & Cemeljic, 2002
- Test setup: ZxR=(500x200)grid cells=(80x20)R_i
- Slower propagation of resistive jet

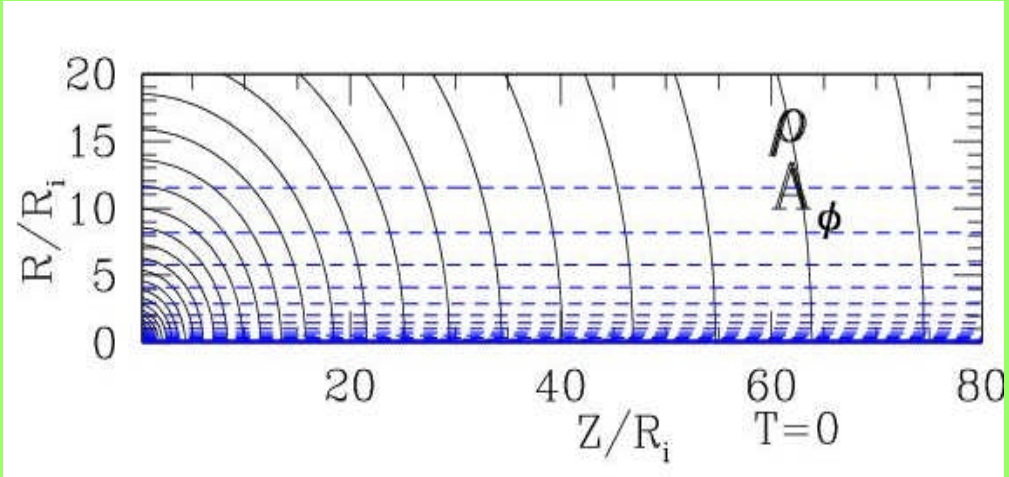

Equations of resistive MHD

$$\frac{\partial \rho}{\partial t} + \nabla \cdot (\rho \mathbf{u}) = 0$$

$$\rho \left[\frac{\partial \mathbf{u}}{\partial t} + (\mathbf{u} \cdot \nabla) \mathbf{u} \right] + \nabla p - \rho \nabla \left(\frac{GM}{\sqrt{r^2 + z^2}} \right) - \frac{\mathbf{j} \times \mathbf{B}}{c} = 0$$

$$\frac{\partial \mathbf{B}}{\partial t} - \nabla \times \left(\mathbf{u} \times \mathbf{B} - \frac{c\mathbf{j}}{\sigma} \right) = 0$$

$$\rho \left[\frac{\partial e}{\partial t} + (\mathbf{u} \cdot \nabla) e \right] + p(\nabla \cdot \mathbf{u}) - \frac{\mathbf{j}^2}{\sigma} = \mathbf{0}$$

$$\nabla \cdot \mathbf{B} = \mathbf{0}$$

$$\frac{4\pi}{c} \mathbf{j} = \nabla \times \mathbf{B}$$

$$p = K \rho^{\gamma}, \; e = \frac{p}{\gamma - 1}, \; \gamma = \frac{5}{3}$$

- Magnetic diffusivity η

$$\frac{\partial \mathbf{B}}{\partial t} = \nabla \times (\mathbf{u} \times \mathbf{B}) + \eta \nabla^2 \mathbf{B}, \quad \eta = \frac{c^2}{4\pi\sigma}$$

With polytropic approximation

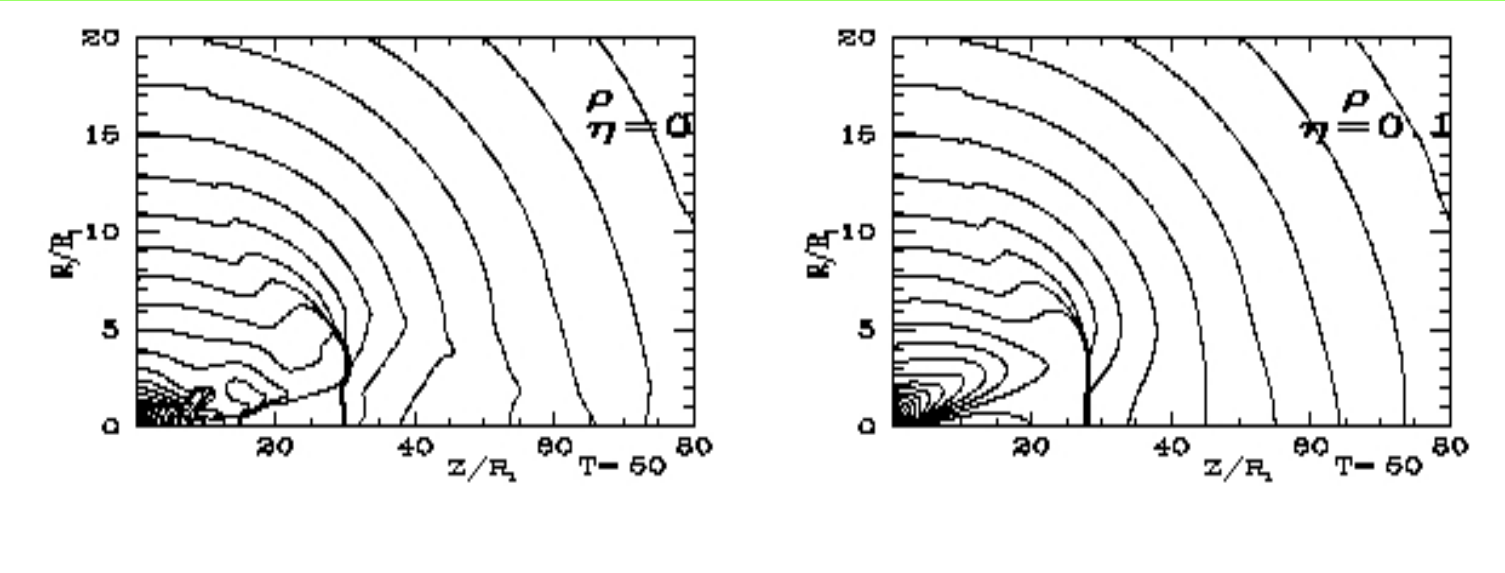

- Result: **Slower propagation of resistive jet**
- But: Irreversible processes forbidden in polytropic approach = shock forming prevented

Energy equation solved

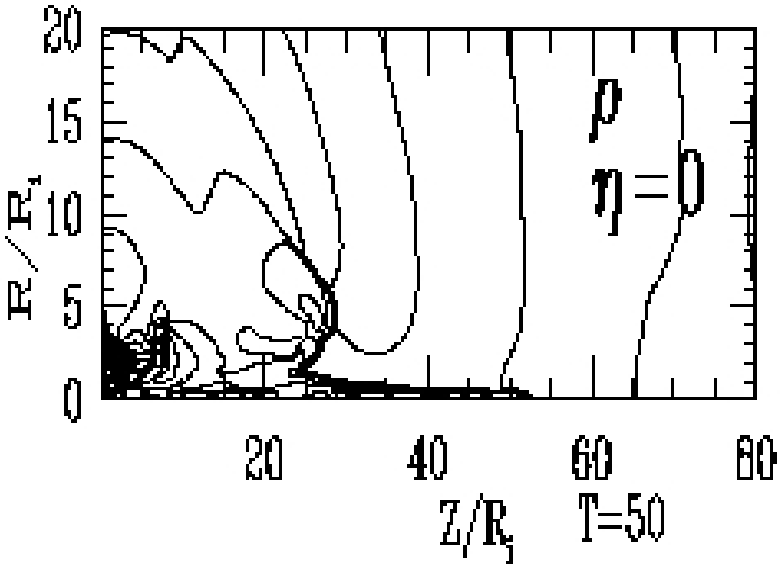

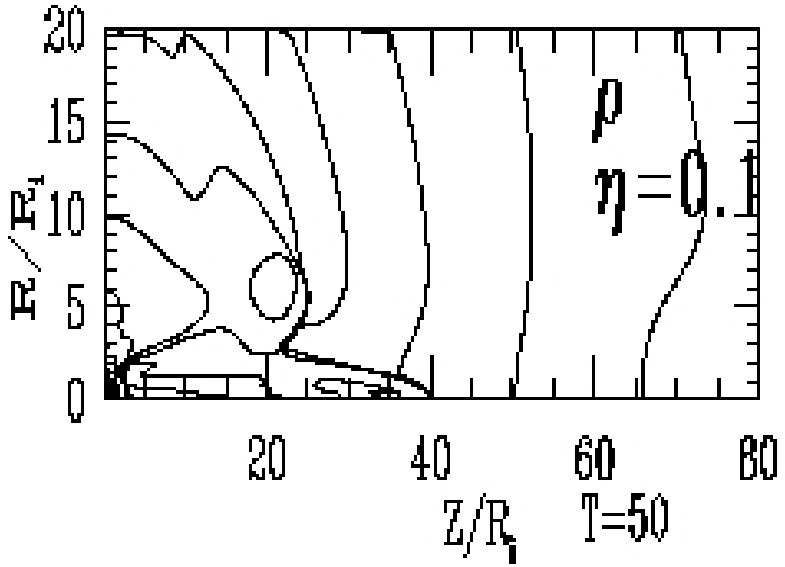

- **Slower propagation of resistive jet**
- Caveat: some features might be boundary-condition dependent
- RESULTS:
- 1) Threshold of numerical resistivity η=0.001
- 2) Difference in the jet front shock position: ΔZ=2.5 Z/R_i

Physics or “art”

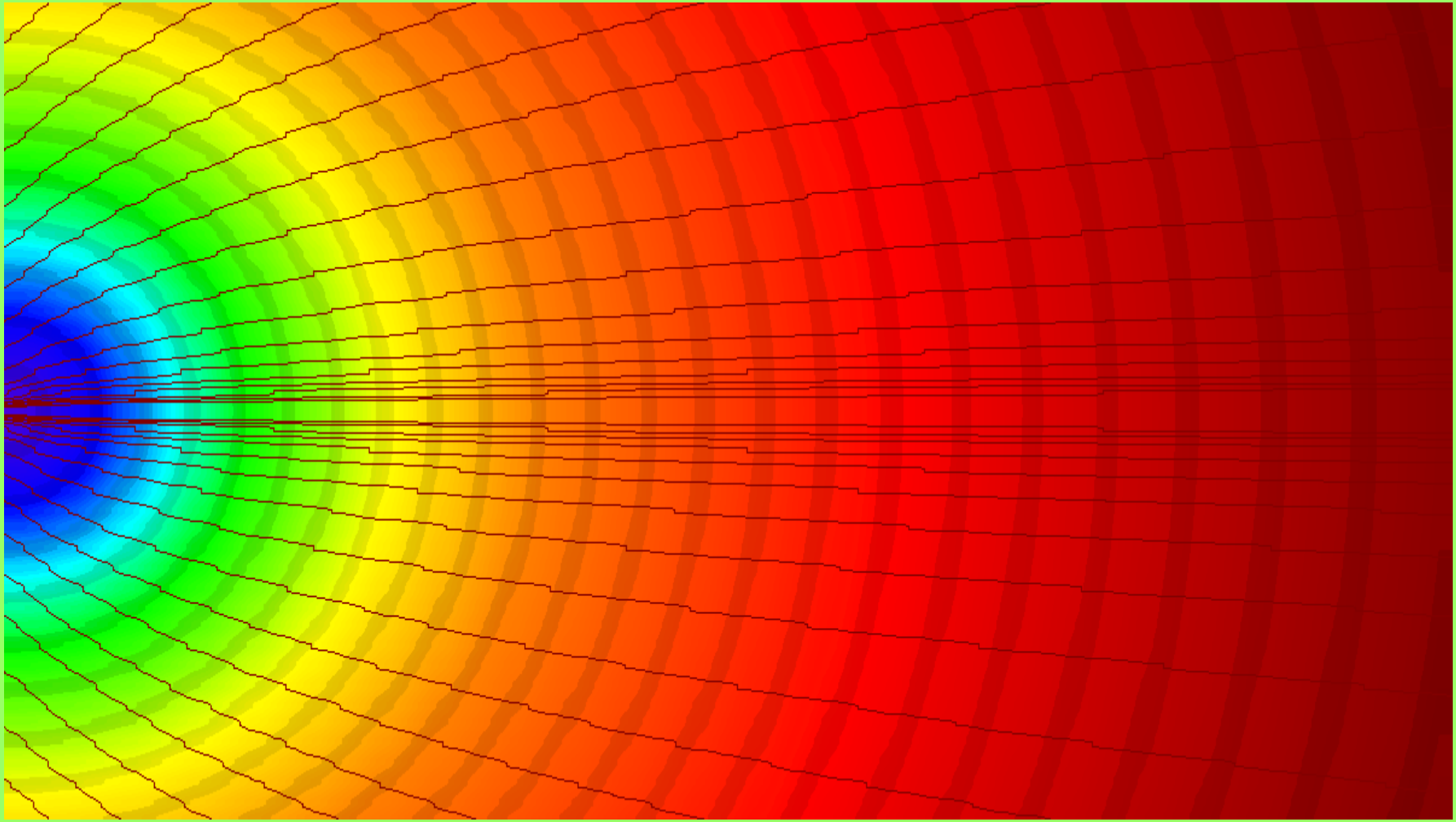

Physics or “art”

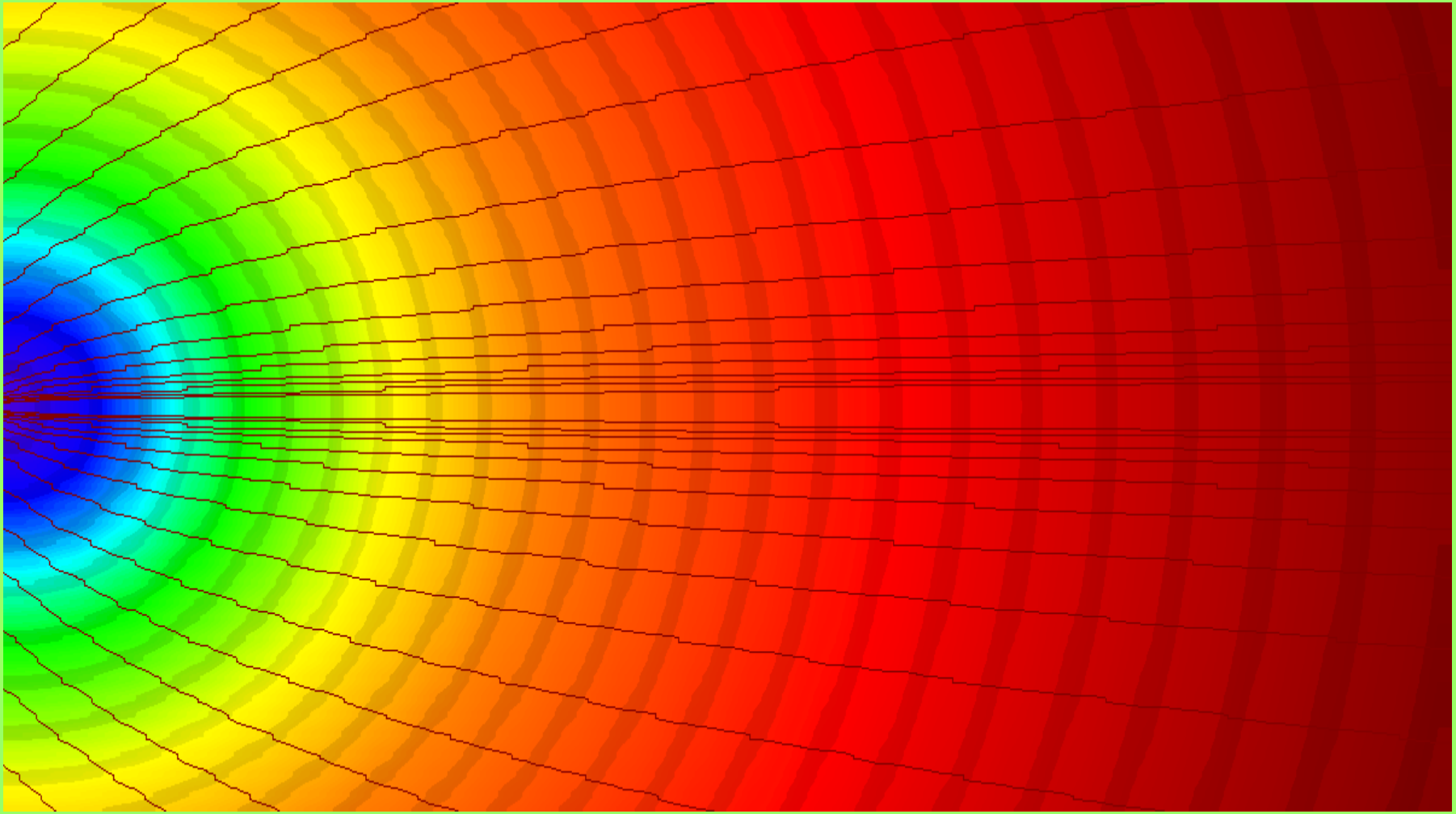

Prospects

- Webpage with the test setups and descriptions
- Test results
- Information about results obtained by each code
- Referees of the papers on new codes demand the particular tests to be performed